Quantum memory for light via a stimulated off-resonant Raman process: Beyond the three-level Λ-scheme approximation

A. S. Sheremet, L. V. Gerasimov, I. M. Sokolov, and D. V. Kupriyanov*
Department of Theoretical Physics, State Polytechnic University, 195251 St. Petersburg, Russia

O. S. Mishina, E. Giacobino, and J. Laurat
Laboratoire Kastler Brossel, Université Pierre et Marie Curie, Ecole Normale Supérieure, CNRS, Case 74, 4 place Jussieu, F-75252 Paris, Cedex 05, France
(Received 19 July 2010; published 30 September 2010)

We consider a quantum memory scheme based on the conversion of a signal pulse into a long-lived spin coherence via stimulated off-resonant Raman process. For a storing medium consisting of alkali-metal atoms, we have calculated the Autler-Townes resonance structure created by a strong control field. By taking into account the upper hyperfine states of the D_1 optical transition, we show important deviations from the predictions of the usual three-level Λ-scheme approximation and we demonstrate an enhancement of the process for particular detunings of the control. We estimate the memory efficiency one can obtain using this configuration.

DOI: 10.1103/PhysRevA.82.033838 PACS number(s): 42.50.Gy, 42.50.Ct, 32.80.Qk, 03.67.−a

I. INTRODUCTION

Long-lived and highly efficient quantum memories for light are a crucial tool for quantum information processing, quantum computing, long-distance secure communication, and scalable networks [1,2]. Various physical systems are intensively investigated and many significant advances have been recently reported [3,4]. In particular, large ensembles of identical atoms, as gases at room temperature [5–9] or ultracold samples [10–12], have been successfully used for demonstrating the storage and retrieval of quantum states in different regimes.

In the theoretical investigations of such quantum memories, the description of the light-atoms interface is usually based on a three-level Λ configuration, with two ground states and one excited state [13–15]. However, the hyperfine interaction in the upper states of alkali-metal atoms is not strong enough for the system to be perfectly described by this approximation. The multilevel structure of alkali-metal atoms has thus to be taken into account for a correct description of the quantum memory effect [16,17]. In this article, we show for the D_1 optical transition how an additional level significantly modifies the stimulated Raman process and we finally evaluate the efficiency of pulse storage and retrieval in this configuration.

The article is organized as follows. Section II first introduces the energy diagram and the assumptions on which our work is based. We then present the theoretical model and provide a general expression of the atomic sample susceptibility. In Sec. III, we study the susceptibility behavior for different frequency detunings of the control and probe modes and we explain how the multilevel structure significantly modifies the quantum light transport driven by coherent scattering mechanism in the conditions of electromagnetically induced transparency or stimulated Raman process. In Sec. IV, we present calculations for the transport of a signal pulse in an optically dense sample. The signal pulse is tuned in the spectral region where the Autler-Townes resonance would be maximal in its amplitude and the stimulated Raman scattering would be most effective. The achievable efficiency of a quantum memory protocol performed in this configuration is finally discussed, in both cases of forward and backward retrieval.

II. AUTLER-TOWNES EFFECT IN THE D_1 LINE OF ALKALI-METAL ATOM

In this section, we present the energy configuration under study and we detail the theoretical model used to fully describe this configuration. A general expression of the susceptibility of the medium is finally given.

A. Basic assumptions

In this article we consider the case of alkali-metal atoms and focus in particular on the D_1 optical transition. Figure 1 shows the energy diagram and Fig. 2 shows the excitation geometry. The atoms populate the upper hyperfine sublevel of their ground state with maximal spin projection $\{F_+ = I + 1/2, M = F_+\}$ (where I is atomic nuclear spin) and we denote this state as $|m\rangle$.

The control field has a right-handed circular polarization (σ_+). In this configuration, there is no interaction of the control field with the populated sublevel and only the presence of the probe mode in the orthogonal left-handed circular polarization (σ_-) opens the excitation channel. The probe and control modes coherently couple the populated state $|m\rangle$ with the Zeeman sublevel $\{F_+, M = F_+ - 2\}$ in the ground state, which we denote as $|m'\rangle$, and with two Zeeman sublevels in the excited state $\{F'_- = I - 1/2, M' = F_+ - 1\}$ and $\{F'_+ = I + 1/2, M' = F_+ - 1\}$, which we denote respectively $|n\rangle$ and $|n'\rangle$.

Such a configuration leads to the Autler-Townes (AT) effect [18,19]. As shown in Fig. 1, the energy levels of the excited atomic states $|n\rangle$ and $|n'\rangle$ are modified by the presence of the control field. If the control field is tuned precisely in resonance with the nondisturbed transitions, either $|n\rangle$ or $|n'\rangle$, the interaction with the control mode splits the originally degenerate system of the atomic and field oscillators into two quasienergy sublevels. However, the interaction of the control

*kupr@dk11578.spb.edu

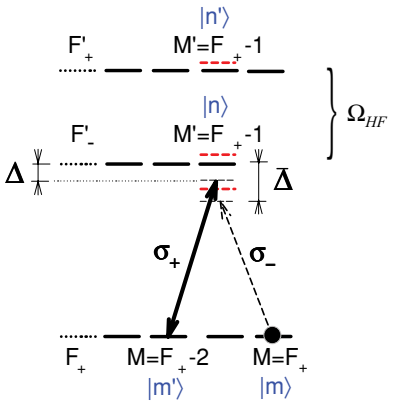

FIG. 1. (Color online) Energy levels and excitation channels considered for the D_1 line of alkali-metal atoms. The atoms populate the upper hyperfine sublevel of their ground state. The system is dressed by a strong control field with a right-handed circular polarization (σ_+) and a frequency detuning Δ. The system is probed by a weak mode with left-handed circular polarization (σ_-) and frequency detuning $\bar{\Delta}$. The three Autler-Townes resonances (AT triplet) are shown by the red dashed lines.

with the other upper hyperfine atomic state is not negligible and the presence of the control mode affects on the locations of both the hyperfine resonances. For an arbitrary detuning of the control, we refer to the joint atom-field quasienergies as the AT triplet (instead of the usual AT doublet) resonance structure. The location of these three resonances for a particular detuning of the control mode is shown by the dashed red lines in Fig. 1.

Let us note finally that the Λ-scheme approximation is the asymptotic limit of our approach: in this limit, the hyperfine interaction is considered to be much stronger than either the natural decay rate γ, the Rabi frequency of the control mode, or the detuning Δ. We will show the limit of this widely used approximation via the full calculation of the AT structure for the D_1 line of ^{133}Cs atom, which has the largest hyperfine splitting among alkali-metal atoms $\Omega_{\mathrm{HF}} = 1168$ MHz $= 256\,\gamma$.

B. Calculation approach

We now turn to our theoretical model. The AT resonance structure can be observed by passing a probe pulse through the sample that will excite the atoms from the populated state $|m\rangle$. The propagation of the probe mode through the medium, in the geometry shown in Fig. 2, is described by the standard macroscopic Maxwell equation, where the dielectric

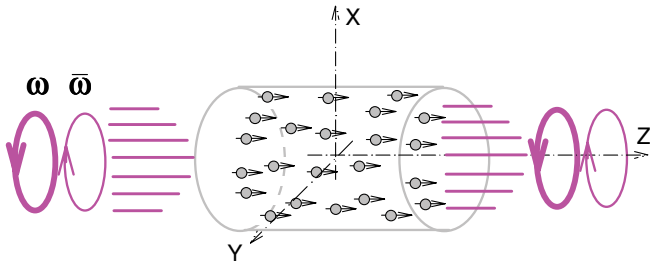

FIG. 2. (Color online) Schematic diagram showing the excitation geometry for the transitions specified in Fig. 1.

susceptibility of the medium, being linear in response to the probe mode, accumulates all the orders of nonlinearities for the control mode. Due to the linearity for the probe field, we can consider an arbitrary set of probe field frequencies forming the signal pulse and we follow the temporal and spatial dynamics of this pulse in a finite sample. The dynamics of the signal pulse and control mode come from the characteristics of the stimulated Raman process, as shown in Refs. [19,20]. The absorption and dispersion parts of the AT resonances in the sample susceptibility result from the combined action of this process on the signal pulse transport.

The positive frequency component $\mathcal{E}^{(+)}(\mathbf{r},t)$ of the signal pulse can be described by a wave packet propagating along the direction z, with a carrier frequency $\bar{\omega}$ and wave number $\bar{k} = \bar{\omega}/c$, such as:

$$\mathcal{E}^{(+)}(\mathbf{r},t) = \epsilon(z;t)e^{-i\bar{\omega}t+i\bar{k}z}. \tag{2.1}$$

For the sake of simplicity the transverse profile of the wave packet is not taken into account, and we thus ignore any diffraction and transverse inhomogeneity of the atomic sample during the propagation process. However, let us point out that the analysis could be generalized for an inhomogeneous system as well.

We then make use of the Fourier expansion of the slow-varying amplitude $\epsilon(z;t)$ of the probe field:

$$\epsilon(z;\Omega) = \int_{-\infty}^{\infty} dt\, e^{i\Omega t}\epsilon(z;t). \tag{2.2}$$

The Fourier component $\epsilon(z;\Omega)$ obeys the following Maxwell equation:

$$\left[-i\frac{\Omega}{c} + \frac{\partial}{\partial z}\right]\epsilon(z;\Omega) = 2\pi i\frac{\bar{\omega}}{c}\,\tilde{\chi}(z;\Omega)\,\epsilon(z;\Omega), \tag{2.3}$$

where $\tilde{\chi}(z;\Omega)$ is the Fourier component of the sample susceptibility. The spectral dependence of the sample susceptibility is shifted by the carrier frequency such that

$$\tilde{\chi}(z;t-t') = e^{i\bar{\omega}(t-t')}\chi(z;t-t'), \tag{2.4}$$

where $\chi(z;t-t')$ is the kernel of the susceptibility operator standardly defined in time representation and determining response of the polarization wave at time t on the driving signal wave (2.1) considered at retarded time $t' < t$.

The susceptibility of the medium is then given by the following expansion:

$$\begin{aligned}\tilde{\chi}(z;\Omega) = &-\sum_{n_1=n,n'}\sum_{n_2=n,n'}\frac{1}{\hbar}\,(\mathbf{d}\cdot\mathbf{e})^*_{n_1m}\,(\mathbf{d}\cdot\mathbf{e})_{n_2m}\\ &\times\int\frac{d^3p}{(2\pi\hbar)^3}n_0(z)\,f_0(\mathbf{p})\\ &\times G^{(--)}_{n_1n_2}\left(\mathbf{p}_\perp, p_z+\hbar\bar{k};\hbar(\bar{\omega}+\Omega)+\frac{p^2}{2m}\right).\end{aligned} \tag{2.5}$$

We have used the following notations: the transition matrix elements of the dipole operator $\mathbf{d}$ are projected onto the polarization vector of the probe mode $\mathbf{e}$, $n_0(z)$ is the density distribution of atoms, and $f_0(\mathbf{p})$ is their momentum distribution, normalized such as

$$\int\frac{d^3p}{(2\pi\hbar)^3}\,f_0(\mathbf{p}) = 1. \tag{2.6}$$

The spectral behavior of the susceptibility (2.5) is determined by the spectral properties of the contributing Green's functions $G^{(--)}_{n_1 n_2}$, describing the dynamics of the upper atomic states dressed by the control mode. The derivation details and precise definitions of the Green's function, matrix elements, etc., are given in the Appendix. We point out here that these functions for all possible $n_1 = n,n'$ and $n_2 = n,n'$ built the 2×2 matrix so the expansion (2.5) consists of four terms. Two diagonal terms asymptotically (for highly resolved hyperfine structure) reproduce the Λ-scheme results for either upper state $|n\rangle$ or $|n'\rangle$. The two others terms, which are interference terms, significantly modify the predictions of the Λ-scheme approximation, as we will show in the following.

III. SPECTRAL BEHAVIOR OF THE SAMPLE SUSCEPTIBILITY

In the case of monochromatic excitation, it is convenient to analyze the Fourier component of the dielectric susceptibility as a function of either its carrier frequency $\bar{\omega}$ or its detuning $\bar{\Delta} = \bar{\omega} - \omega_0$ from the atomic resonance frequency ω_0. In this section we present our calculation of the sample susceptibility $\chi = \chi(\bar{\Delta}) = \chi'(\bar{\Delta}) + i\chi''(\bar{\Delta})$, which were obtained for an homogeneous medium consisting of ^{133}Cs atoms. We assume a typical configuration of magneto-optical trap (MOT) such that the effects of atomic motion on the time scale of a few microseconds can be disregarded.

In the following, the susceptibility given by Eq. (2.5) will be scaled in units of $n_0 \lambda\!\!\!^{-3}$, where n_0 is the density of atoms and $\lambda\!\!\!^{-} = \lambda/2\pi$. In typical MOT conditions, the atomic gas is dilute and $n_0 \lambda\!\!\!^{-3} \ll 1$ but the sample can be optically thick if $n_0 \lambda\!\!\!^{-2} L \gg 1$, where L is the sample length. It is very important to underline that the transition matrix elements $V_{nm'}$ and $V_{n'm'}$, contributing to the Green's functions given by Eqs. (A4) and (A5), cannot be considered as independent parameters. They are expressed by one reduced matrix element multiplied by two different, but dependent, algebraic factors, which are determined by an electronic and nuclear coupling scheme in the upper hyperfine states and by the polarization of the exciting field. As an external characteristic of the coupling strength with the control mode, we use the Rabi frequency $\Omega_c = 2|V_{nm'}|/\hbar$ defined with respect to the lower energy transition. The results of our calculations will be compared with the usual Λ scheme where only state $|n\rangle$ is taken into consideration.

Figure 3 gives the spectral dependencies for imaginary (absorption) and real (dispersion) components of the susceptibility $\chi(\bar{\Delta})$ (scaled in units of $n_0 \lambda\!\!\!^{-3}$) for a Rabi frequency $\Omega_c = 15\gamma$ and for the control field on resonance with the atomic transition $\Delta = 0$. In these conditions, there is no light absorption in the medium. The imaginary part of the susceptibility is responsible for the losses caused by incoherent scattering. All three AT components are shown as well as the doublet approximation calculated in the three-level Λ model when the upper state $|n'\rangle$ is disregarded. At first sight, the discrepancy between the exact result and the Λ-scheme approximation seems small. However, two important qualitative differences can be pointed out.

First, in the multilevel configuration, the spectral point, where due to electromagnetically induced transparency (EIT) the absorption falls down to its minimum level, is shifted to

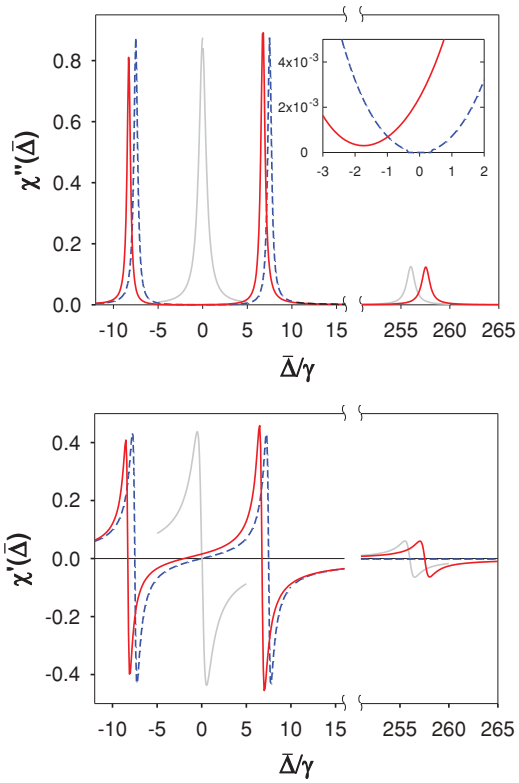

FIG. 3. (Color online) Absorption part (upper panel) and dispersion part (lower panel) of the sample susceptibility in the presence of the control field tuned in resonance with the atomic transition ($\Delta = 0$), for a Rabi frequency $\Omega_c = 15\gamma$. The susceptibility components are scaled by $n_0 \lambda\!\!\!^{-3}$. Red solid curves show the result of the exact calculations and blue dashed curves are plotted for the usual Λ-scheme approximation. For reference, gray curves give the profiles of the atomic resonances without control field. As shown in the inset of the upper panel, the EIT resonance is shifted to the red and the medium looses its perfect transparency at this point.

the red and the EIT resonance does not occur for $\bar{\Delta} = \Delta$, as it always does in the case of the Λ model. As clearly shown in the inset of Fig. 3, the light shift is significant and it depends on the Rabi frequency of the control field. This light shift was first observed by Hau and co-workers in the pioneering experiment on slow light [21]. Second, the medium does not have a perfect transparency at the optimal EIT point as it also always does for the Λ-scheme approximation. In our example this effect seems rather weak, but it is nonvanishing, even in the limit of $\Omega_c \to 0$, and it can become important if the medium has a very large optical depth, where the losses caused by incoherent scattering can accumulate [22].

In Fig. 4, the absorption and dispersion parts of the sample susceptibility are shown for two detunings of the control mode: $\Delta = -50\gamma$ and $\Delta = 50\gamma$. For both detunings, the lines close to the atomic resonances are only slightly disturbed by the control field and we show only the part of the spectral domain where $\bar{\Delta} \sim \Delta$. We compare the profile of the AT resonance located near the frequency of the control mode with predictions of the Λ-scheme approximation. The dependencies of Fig. 4 show much larger deviation with the calculations based on the Λ scheme than in the situation of Fig. 3. This is a direct consequence of the fact that the detuning Δ is

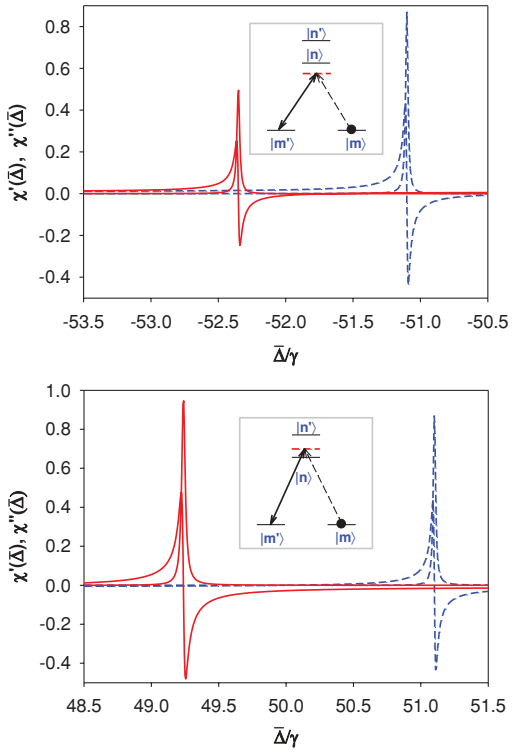

FIG. 4. (Color online) Same as in Fig. 3 but for two different detunings. The upper panel corresponds to $\Delta = -50\gamma$ and the lower panel to $\Delta = 50\gamma$. Only one component of the AT triplet, which is located near $\bar{\Delta} \sim \Delta$, is shown.

comparable with the hyperfine interaction between electronic angular momentum and nuclear spin.

If the hyperfine interaction was negligible, which asymptotically occurs when one moves the AT resonance either much lower than state $|n\rangle$ or much higher than state $|n'\rangle$, then the considered scheme would be equivalent to the excitation of an atom with the nuclear spin decoupled from the electronic angular momentum, which has one-half value. The considered Λ-type interaction between the ground-state Zeeman sublevels is impossible in this case. This explains why, when the detuning Δ is not negligible with respect to the hyperfine splitting Ω_{HF} (here $\Delta = -50\gamma = -\Omega_{\mathrm{HF}}/5.12$), the amplitude of the AT resonance, shown in the upper panel of Fig. 4 is reduced as compared to the value given by calculations based on the Λ-scheme model. On the other hand, both models show approximately the same narrowing of the resonance linewidth with increasing of Δ. More generally modifications of the AT resonance in the vicinity of either D_1 or D_2 transition due to the interplay between the hyperfine interaction and the optical detunings have a strong impact on observation of the EIT effect in the hot atomic gas and will be discussed in detail in Ref. [22].

The situation changes if the control mode is tuned between the hyperfine components as shown in the lower panel of Fig. 4 for $\Delta = +50\gamma$. One can observe an enhancement of the AT effect in comparison with predictions of the Λ-scheme approximation. This enhancement is even slightly larger for the dispersion component, as it is more sensitive to the interference terms contributing into the sample susceptibility [see Eqs. (2.5) and (A4)]. As a consequence the signal pulse passing through the atomic ensemble can undergo longer delay at the output than it would be expected from the Λ-scheme model. This constitutes an interesting advantage when the Raman process is applied to a quantum memory protocol in this configuration. This is detailed in the next section.

IV. APPLICATION TO QUANTUM MEMORY

As shown before, the Raman configuration with positive detuning may lead to an improvement for the storage of a signal pulse. We evaluate here the performances of a memory in this particular case, where the control mode is tuned between the upper state hyperfine levels. In all the following, the Rabi frequency of the control mode is $\Omega_c = 15\gamma$ and it is detuned by $\Delta = 50\gamma$, as in the lower panel of Fig. 4.

A. Delay of the pulse transport in the atomic sample

We consider a coherent pulse with rectangular profile impinging on the sample. Using Eqs. (2.5) and (2.3) we can calculate the shape of the outgoing pulse for various situations. We have considered here three signal pulses having identical shape but different carrier frequencies. This approach allows to model a multimode situation where we make a discrete Fourier expansion with frequencies that are multiples of $2\pi/T$, where T is the pulse duration. In the following, we use a dimensionless amplitude for the signal field denoted by $\alpha(z,t)$. We assume input pulses with rectangular profile, such that $\alpha_{\mathrm{in}}(t) = \theta(t) - \theta(t-T)$, where $\theta(t)$ is the step function, $\theta(t) = 1(t > 0)$ or $= 0\,(t < 0)$. Figure 5 shows how this pulse is delayed and how its shape is modified after passing through the atomic medium.

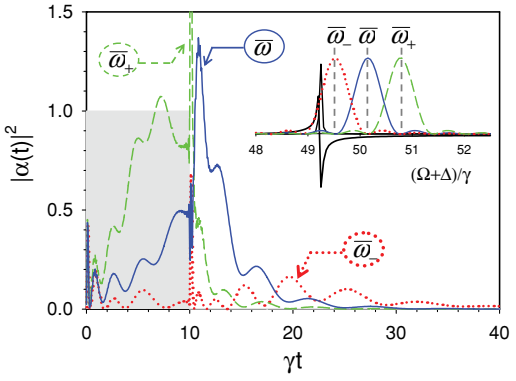

FIG. 5. (Color online) Time dependence of the outgoing signal pulses. The time $t = 0$ corresponds to the arrival of the incoming pulse front to the atomic medium. For the reference, the gray box gives the outgoing pulse in the absence of atomic medium. Three pulses with the same duration $T = 10\gamma^{-1}$ but different carrier frequencies $\bar{\omega}_-$, $\bar{\omega}$, and $\bar{\omega}_+$, where $\bar{\omega}_\pm$ are shifted by $\pm 2\pi/T$, propagate through the optically thick sample with an optical depth $n_0 \lambda^2 L = 50$. The inset shows the pulse spectra with respect to the AT resonance. The $\bar{\omega}_-$ pulse (red dotted line) experiences the longest delay but also the largest level of losses due to incoherent scattering. The $\bar{\omega}_+$ pulse (green dashed line) has the lowest level of losses but also the smallest delay. The central pulse has an intermediate carrier frequency and corresponds to a balance between the losses and delay.

As shown in the inset of Fig. 5, the central pulse has a carrier frequency $\bar{\omega}$ chosen to ensure some balance between transparency and delay. The two other pulses are shifted by $\pm 2\pi/T$, with $\bar{\omega}_{\pm} = \bar{\omega} \pm 2\pi/T$, which makes them spectrally orthogonal to the central mode. By extrapolating these series to infinite number of modes ($\bar{\omega}_q = \bar{\omega} + 2\pi q/T$, where $q = 0, \pm 1, \pm 2, \ldots$) we can extract the complete set of Fourier modes and use them for the expansion of an input signal pulse of arbitrary temporal profile with sharp bound. Such a Fourier description of an arbitrary pulse of a finite duration T allows one to follow the transformation of each spectral component in the output and could be important for the multimode quantum information processing.

The delay of the pulse propagating through the optically dense medium of length L strongly depends on the optical depth. For a monochromatic signal mode at frequency $\bar{\omega}$ the optical depth $b(\bar{\omega})$ is given by

$$b(\bar{\omega}) = 4\pi\chi''(\bar{\omega})\frac{L}{\lambda}. \tag{4.1}$$

The depth varies from $b(\bar{\omega}) \gg 1$ near the points of the AT resonances to $b(\bar{\omega}) \ll 1$ in the transparency domains. In the Λ-scheme approximation, the resonance optical depth is defined in a unique way. In the multilevel situation the optical depth at resonance depends on the chosen transition. However, it is always closes to $b_0 \sim n_0\lambda^2 L$, which was taken equal to 50 for the round of calculations presented in Fig. 5.

It can be seen in Fig. 5 that the shape of the outgoing pulses is strongly modified as compared to the initial pulse. First, all three pulses corresponding to $\bar{\omega}$, $\bar{\omega}_+$, and $\bar{\omega}_-$ are delayed. The pulse with frequency $\bar{\omega}_-$, the spectrum of which overlaps the most with the AT peak, spreads over longer times and has a much longer average delay than the other ones. However, this pulse has the highest level of losses due to the incoherent scattering. The pulse with carrier frequency $\bar{\omega}_+$ has a lower level of losses and better preserves the original rectangular shape, but the delay is quite small.

We can interpret the outgoing signal pulses in Fig. 5 in the following way: The part of the pulse going out of the medium at times smaller than the time duration of the original pulse, $T = 10\gamma^{-1}$, corresponds to direct transmission, while the tail of the outgoing pulse, which is emitted after the end of the incoming pulse, corresponds to a potentially stored and recovered signal. This is a good approximation if the transient processes associated with switching off (on) the control mode as well as the retardation effects are negligible. The fact that in off-resonant stimulated Raman scattering the transient processes only weakly interfere with the transport of the signal pulse was verified in Ref. [15].

B. Efficiency of pulse storage and retrieval

We now turn to the full memory protocol, including storage and retrieval stages. The control pulse is switched off when the end front of the incoming signal pulse has entered the sample. After short transient dynamics, the signal wave packet, which is localized in the sample, is mostly converted into a standing spin wave distributed into the whole sample. This spin wave is given by the off-diagonal matrix elements (spin coherence) between Zeeman sublevels m and m' existing in the system at time T, which we denote as $\sigma(z,T)$. To calculate the spin distribution we have applied the theoretical approach developed in Ref. [16] and modified it for the present case by including the dissipation processes. The spin distribution is shown in the upper panel of Fig. 6.

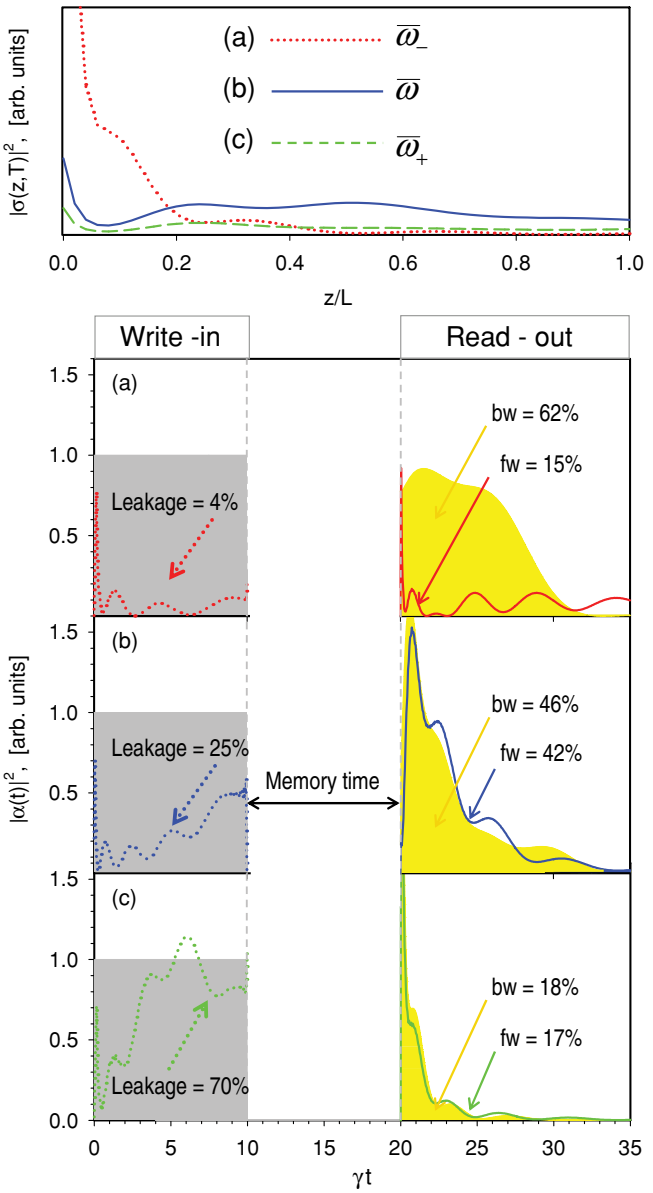

FIG. 6. (Color online) Quantum memory. This figure shows the dynamics of the system for the same parameters as described in Fig. 5. Upper panel shows the spin distribution $\sigma(z,T)$ in the sample at time T ("stored light"). In the lower panel the signal pulse is retrieved on demand after a certain memory time via switching on the control field in either forward (solid lines) or backward (yellow filled area) direction. The leakage of each pulse, which is the light transmitted during the write-in stage, is indicated by the dotted line [(a) the input pulse carrier frequency is $\bar{\omega}_-$, (b) the input pulse carrier frequency is $\bar{\omega}$, and (c) the input pulse carrier frequency is $\bar{\omega}_+$]. The read-out stage is characterized by the memory efficiency for the forward (fw) or backward (bw) retrieval.

After a controllable delay, the spin wave can be converted back into the signal wave packet by sending the second

control pulse. This can be done in either forward or backward directions. In the first case, the retrieved pulse would reproduce the tail of the outgoing signal pulse, the propagation of which was interrupted in the writing stage of the memory protocol. This can be seen by comparing the graphs of Figs. 6 and 5.

The pulse retrieval in the backward direction leads to some advantages. As discussed in Ref. [13], while applying the time-reversal arguments one can expect a higher efficiency for backward retrieval after a round of optimization. Also, the shape of the pulse recovered in the backward direction better reproduces its original profile. Our numerical simulations confirm this statement. The spin distribution for the mode $\bar{\omega}_-$ indicates that the signal is mostly stored near the left bound of the sample. Then it seems more natural to redirect the retrieved pulse in the backward direction where it would have less absorption and, according to time-reversal arguments, would be regenerated by the medium to its original profile. That can be seen in Fig. 6, which shows approximately rectangular retrieved profile for the $\bar{\omega}_-$ mode with efficiency more than 60%.

To conclude this section let us underscore the fact that the predicted quality of the considered memory channel is quite good. The obtained results show that in conditions currently attainable for a MOT the efficiency of the memory protocol could be expected up to 60%. We can expect further improvement in the efficiency by using the optimization of the temporal profile of the input pulse, as described in Refs. [13,23].

V. CONCLUSION

In this article we have considered the propagation of a signal pulse in conditions of stimulated Raman process through a sample of alkali-metal atoms. We have shown that the presence of the hyperfine interaction in the upper state significantly modifies the Autler-Townes effect observed in the D_1 line of such atoms. In particular, we have demonstrated that it is more efficient to tune the control mode between the upper state hyperfine sublevels where the stimulated Raman process is enhanced and provides more effective delay of the signal pulse.

We have analyzed the dynamics of a signal pulse with initial rectangular profile and calculated how such a pulse is delayed and how its shape is modified after passing through the atomic medium. This dynamics reveals that the outgoing pulse is quite sensitive to the detuning of the pulse carrier frequency from the Autler-Townes resonance created by the control field. We have used our results to evaluate the efficiency of a quantum memory protocol based on the same stimulated Raman process. This has been done both for the forward and the backward retrieval schemes. We have shown that the backward retrieval can be more effective and the shape of recovered pulse can better reproduce its original profile. In particular, our results show that in conditions currently attainable for a cesium magneto-optical trap the efficiency of the memory protocol could be expected more than 60%.

ACKNOWLEDGMENTS

This work was supported by RFBR (Grants No. 10-02-00103 and No. 08-02-91355), by Federal Program "Science of innovation Russia on 2009–2013" (Contract No. P2326), and by the EC under the ICT/FET project COMPAS. A.S. and L.G. acknowledge the financial support from the charity Foundation "Dynasty" and O.M. from the Ile-de-France program IFRAF.

APPENDIX: THE ATOMIC GREEN'S FUNCTIONS AND SAMPLE SUSCEPTIBILITY

The atomic Green's functions and sample susceptibility are found in the second quantization formalism using a nonstationary diagram technique [15,24,25]. The Maxwell equation considered in the main text of the article can be expressed by the following diagram equation:

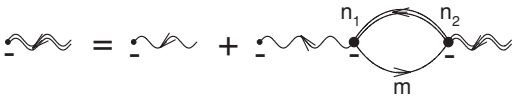

(A1)

Here the double wavy single-ended lines describe the signal field amplitude dressed by the interaction process shown in Fig. 1 when this field propagates through the sample. The single double-ended wavy line is the retarded Green's function for light propagating freely in vacuum. The loop consisting of the atomic Green's functions and the vertices describes the polarization operator or susceptibility of the sample in response to the probe field. For the sake of clarity, we show the internal indices n_1 and n_2 running the quantum numbers of excited atomic states n,n' (Fig. 1).

The retarded-type Green's functions of the excited atomic states dressed by the interaction with the control and vacuum modes and shown as double line in the polarization operator of Eq. (A1) are expressed by the following Dyson equations:

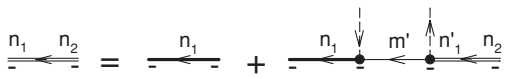

(A2)

The outward and inward directed dashed arrows represent the field amplitude of the control mode and the thick solid line is the retarded-type Green's function of state $|n_1\rangle$ dressed by interaction with the vacuum modes only. This function in the first term in the right side should be multiplied by the factor $\delta_{n_1 n_2}$ (not shown). It is expressed by the diagram equation defining the natural decay rate of the excited state:

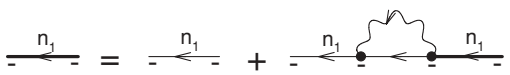

(A3)

The thin solid and wavy lines are respectively nonperturbed vacuum Green's functions of the atom and field.

The minus signs in these diagrams indicate the causal (time-ordered) character in averaging of the operators' product. In the case of field the expectation value is taken over its vacuum state. But in the case of atoms the averaging is taken over the initial state of atomic system. As a consequence, if in the above diagrams the time naturally rises from right to left, the backward directed thin line in the polarization operator (A1) is proportional to the density of atoms in the initially populated state $|m\rangle$. The diagrams (A1)–(A3) can be interpreted as a graphical solution of the Bloch equations in the first-order response to the signal field.

If the control mode is monochromatic then after Fourier transform the integral equations (A2) can be written in a form

of algebraic equations. These equations give us the set of four Green's functions $G^{(--)}_{n_1 n_2}(\mathbf{p},E)$ defined in the reciprocal space. These functions contribute into equation (A1) with the "on shell" energy argument, which is given by $E = \hbar(\bar{\omega}+\Omega) + p^2/2m_0$, i.e., is expressed by the kinetic energy of atom $p^2/2m_0$ ($\mathbf{p}$ and m_0 are atomic momentum and mass, respectively; the internal ground-state energy is considered as zero level) plus the energy of a photon from the signal field $\hbar(\bar{\omega}+\Omega)$. Let us point out that because of the momentum conservation in the polarization operator the momentum of excited atom $\mathbf{p}'$ is shifted from $\mathbf{p}$ by the momentum of absorbed signal photon such that $p'_z = p_z + \hbar\bar{k}$.

The Green's functions have the following analytical expression:

$$G^{(--)}_{nn}(\mathbf{p},E) = \hbar\left\{E - \frac{p^2}{2m_0} - E_n + i\hbar\frac{\gamma}{2} - \frac{|V_{nm'}|^2\left[E - \frac{p^2}{2m} - E_{n'} + i\hbar\frac{\gamma}{2}\right]}{[E - E_{n'+}(\mathbf{p},\omega)][E - E_{n'-}(\mathbf{p},\omega)]}\right\}^{-1},$$

$$G^{(--)}_{n'n}(\mathbf{p},E) = \frac{V_{n'm'}V^*_{nm'}}{[E - E_{n'+}(\mathbf{p},\omega)][E - E_{n'-}(\mathbf{p},\omega)]} \times G^{(--)}_{nn}(\mathbf{p},E)\ldots. \tag{A4}$$

Two other functions can be similarly written via transposing the indices $n \Leftrightarrow n'$.

The following notation is used: $V_{nm'} = (\mathbf{d}\cdot\mathbf{E})_{nm'}$, $V_{n'm'} = (\mathbf{d}\cdot\mathbf{E})_{n'm'}$ are the matrix elements of interaction with the control field; $\mathbf{E}$ is the complex amplitude of the field's positive frequency component $\mathbf{E}^{(+)}(\mathbf{r},t) = \mathbf{E}\exp(-i\omega t + i\mathbf{k}\cdot\mathbf{r})$; E_n, $E_{n'}$ are nonperturbed energies of the excited states; and γ is the natural decay rate of the excited state. The quasienergies in the denominators of Eqs. (A4) contribute to the excitation spectrum dressed by interaction with vacuum modes and control field while the hyperfine interaction is infinitely strong. They are given by

$$E_{n\pm}(\mathbf{p},\omega) = E_{m'} + \frac{\mathbf{p}^2}{2m_0} + \frac{\hbar}{2}\left[\omega - \frac{\mathbf{k}\cdot\mathbf{p}}{m_0} + \omega_{nm'} - i\frac{\gamma}{2}\right] \pm \left[|V_{nm'}|^2 + \frac{\hbar^2}{4}\left(\omega_{nm'} - \omega + \frac{\mathbf{k}\cdot\mathbf{p}}{m_0} - i\frac{\gamma}{2}\right)^2\right]^{1/2} \tag{A5}$$

and similarly for n'. Here $E_{m'}$ is the energy of state $|m'\rangle$, which for the system of degenerate Zeeman sublevels shown in Fig. 1 coincides with the energy of state $|m\rangle$, such that $E_{m'} = E_m = 0$. Quasienergies (A5) are convenient intermediate parameters describing the AT structure if only one state either $|n\rangle$ or $|n'\rangle$ is taken into consideration. But actual location of the AT poles is described by full susceptibility of the sample given by Eq. (2.5), where all four Green's functions equally contribute.

[1] H. J. Kimble, Nature (London) **453**, 1023 (2008).
[2] K. Hammerer, A. S. Sørensen, and E. S. Polzik, Rev. Mod. Phys. **82**, 1041 (2010).
[3] Christoph Simon *et al.*, Eur. Phys. J. D **58**, 1 (2010).
[4] A. I. Lvovsky, B. C. Sanders, and W. Tittel, Nat. Photon. **3**, 706 (2009).
[5] M. D. Eisaman *et al.*, Nature (London) **438**, 837 (2005).
[6] I. Novikova, A. V. Gorshkov, D. F. Phillips, A. S. Sørensen, M. D. Lukin, and R. L. Walsworth, Phys. Rev. Lett. **98**, 243602 (2007).
[7] J. Cviklinski, J. Ortalo, J. Laurat, A. Bramati, M. Pinard, and E. Giacobino, Phys. Rev. Lett. **101**, 133601 (2008).
[8] J. Appel, E. Figueroa, D. Korystov, M. Lobino, and A. I. Lvovsky, Phys. Rev. Lett. **100**, 093602 (2008).
[9] G. Hétet, M. Hosseini, B. M. Sparkes, D. Oblak, P. K. Lam, and B. C. Buchler, Opt. Lett. **33**, 2323 (2008).
[10] T. Chanelière *et al.*, Nature (London) **438**, 833 (2005).
[11] K. S. Choi *et al.*, Nature (London) **452**, 67 (2008).
[12] K. Honda, D. Akamatsu, M. Arikawa, Y. Yokoi, K. Akiba, S. Nagatsuka, T. Tanimura, A. Furusawa, and M. Kozuma, Phys. Rev. Lett. **100**, 093601 (2008).
[13] A. V. Gorshkov, A. André, M. Fleischhauer, A. S. Sørensen, and M. D. Lukin, Phys. Rev. Lett. **98**, 123601 (2007); A. V. Gorshkov, A. André, M. D. Lukin, and A. S. Sørensen, Phys. Rev. A **76**, 033805 (2007); **76**, 033806 (2007); A. V. Gorshkov, T. Calarco, M. D. Lukin, and A. S. Sørensen, *ibid.* **77**, 043806 (2008).
[14] J. Nunn, K. Reim, K. C. Lee, V. O. Lorenz, B. J. Sussman, I. A. Walmsley, and D. Jaksch, Phys. Rev. Lett. **101**, 260502 (2008).
[15] O. S. Mishina, N. V. Larionov, A. S. Sheremet, I. M. Sokolov, and D. V. Kupriyanov, Phys. Rev. A **78**, 042313 (2008).
[16] O. S. Mishina, D. V. Kupriyanov, J. H. Müller, and E. S. Polzik, Phys. Rev. A **75**, 042326 (2007).
[17] O. S. Mishina, A. S. Sheremet, N. V. Larionov, and D. V. Kupriyanov, Opt. Spectrosc. **108**, 313 (2010).
[18] S. H. Autler and C. H. Townes, Phys. Rev. **100**, 703 (1955).
[19] V. S. Letokhov and V. P. Chebotaev, *Nonlinear Laser Spectroscopy* (Springer-Verlag, Berlin, 1977).
[20] K. Surmacz, J. Nunn, F. C. Waldermann, Z. Wang, I. A. Walmsley, and D. Jaksch, Phys. Rev. A **74**, 050302(R) (2006).
[21] L. V. Hau, S. E. Harris, Z. Dutton, and C. H. Behroozi, Nature (London) **397**, 594 (1999).
[22] O. Mishina *et al.* (unpublished).
[23] I. Novikova, N. B. Phillips, and A. V. Gorshkov, Phys. Rev. A **78**, 021802 (2008).
[24] L. V. Keldysh, Zh. Eksp. Teor. Fiz. **47**, 1515 (1964) [Sov. Phys. JETP **20**, 1018 (1965)].
[25] E. M. Lifshits and L. P. Pitaevskii, in *Physical Kinetics, Course of Theoretical Physics* (Pergamon Press, Oxford, 1981), Vol. 10.